Explicitly Multimodal Benchmarks for Multi-Objective Optimization

Ryosuke Ota[1], Reiya Hagiwara[1], Naoki Hamada[2], Likun Liu[1], Takahiro Yamamoto[3], and Daisuke Sakurai[1]

[1]Kyushu University
[2]KLab, Inc.
[3]Tokyo Gakugei University

February 13, 2024

Abstract

In multi-objective optimization, designing *good* benchmark problems is an important issue for improving solvers. Controlling the global location of Pareto optima in existing benchmark problems has been problematic, and it is even more difficult when the design space is high-dimensional since visualization is extremely challenging. As a benchmarking with explicit local Pareto fronts, we introduce a benchmarking based on basin connectivity (3BC) by using basins of attraction. The 3BC allows for the specification of a multimodal landscape through a kind of topological analysis called the basin graph, effectively generating optimization problems from this graph. Various known indicators measure the performance of a solver in searching global Pareto optima, but using 3BC can make us localize them for each local Pareto front by restricting it to its basin. 3BC's mathematical formulation ensures the accurate representation of the specified optimization landscape, guaranteeing the existence of intended local and global Pareto optima.

1 Introduction

Benchmark problems for multi-objective optimization help evaluate and understand its solvers. A good benchmark problem would reveal solver behaviors in different situations, hinting their performance. In the literature of evolutionary computation, for example, we can find a number of famous benchmark suites. The property of multi-objective optimization problems we mainly consider is multimodality. Although a clear consensus on what constitutes multimodality is hardly reached, a key characteristic is the basins of attraction that trap solvers, making them fail to explore global optima [18]. (See section 2.1 for more.)

In conventional multimodal multi-modal benchmarks, it is difficult to arrange the number and location of local Pareto fronts. Commonly used benchmark problems in section 2.3 use similar constructions as used in Deb's toolkit [5]. This method, which uses several functions combined to form the objective function, may control the Pareto optima locally but cannot globally. That is, it may be possible to make a particular point Pareto optimum by modifying the constituting functions, but then an extra Pareto optimum will arise or disappear at another location. Hence, in order to find reference points, it is a standard way to run algorithms to numerous generations with a large population size, which is imprecise. Although there have been benchmark problems with this goal, specifying the local Pareto fronts, while avoiding unintended ones, remains a significant challenge. When the design space becomes high dimensional, the problem intensifies since visualization becomes extraordinarily challenging.

In this article, we propose a novel benchmark problem named the Benchmarking Based on Basin Connectivity (3BC), in which the user can completely specify the number and location of local Pareto fronts, by using basins of attractions [19]. Therefore, the reference points for all local Pareto fronts can be analytically obtained and it makes it possible to compute performance indicators for each local Pareto front following a rigorous formulation. See section 7 (fig. 13 in particular) for our demonstration.

The 3BC allows the benchmark designer to specify the multimodal landscape, which we model employing the topological analysis of preimage f^{-1}. The designer can specify how the basins of attractions in the landscape connect to each other using a graph we name the *basin graph* (the *reachability graph* [1] is a similar yet more complex variant of our basin graph). The 3BC generates an instance of multi-objective optimization problem from the basin graph. As a first step in our research direction, the 3BC considers 2 objective functions. However, the authors believe the approach is generalizable to benchmarking with more objective functions.

While various indicators can measure the performance of solvers, they mainly focus only on the global Pareto optima since the local Pareto optima are generally unknown in practice. In the paper, however, we can define some basin-wise versions since the local Pareto optima are specified in the 3BC and we can use the basin of each local Pareto optimum. In other words, by computing indicators only in the basin for a local Pareto optimum, we can measure the ability of solvers to search for that local Pareto optimum.

Before this work, multimodality has been inferred usually by clustering the population of evolutionary algorithms. One major problem here, however, is that the induced multimodality has ambiguity: it can vary significantly depending on parameters, including the initial condition, and even random numbers picked for the clustering computation.

Due to its mathematical formulation, the 3BC guarantees the modeled landscape to match the output. That is, the specified local and global Pareto optima exist, forming specified landscapes, and there is no other optima.

2 Related work

2.1 Multimodality model

As mentioned, we regard the key property of multimodality to be the difficulty for a greedy algorithm to find global optima. Finding a satisfactory formal definition, however, has been challenging.

One common definition of multimodality is that a multi-objective optimization problem has local Pareto optima that are not global optima. Li et al. [16] provide a nice review. The problem with this definition is that a multimodal problem in this sense can be solved with a greedy algorithm at times, which is contrary to the ideal of multimodality.

Huband et al. [9] considered the multimodality of each objective function. However, there exist optimization problems that satisfies this condition and can still be solved in a greedy manner. Figure 1 gives such an example. Here, the orange objective function is by itself a multimodal objective with two pits. However, the Pareto optimization, that also optimizes the blue objective function, gives a Pareto set that consists of the green region, local optima, and the red region, the global ones. In such a situation, a greedy solver that follows the local optima can easily reach the global optima, which is contrary to the concept of multimodality.

According to Kerschke et al. [15], multimodality is to have multiple connected components of the local Pareto sets. In the example shown in fig. 1, the orange and blue lines are the graphs of two functions consisting of the two-objective function of one valuable. Each point in the green area is a local (but not global) Pareto point but the local Pareto set consists of one connected component.

This is the base of our multimodality model. Notice, however, that the multimodality as defined by Kerschke et al. [15] can be discussed only when we are talking about points in Pareto optima, not in the whole design space. We thus extend it so that any point in the design space can be given a modality. We do so in the form of basins of attraction.

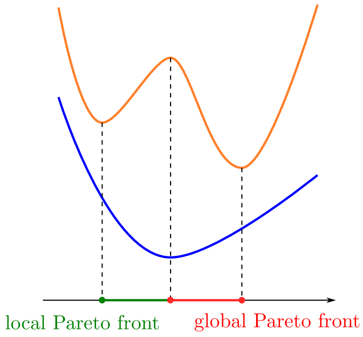

Figure 1: A 2-objetive function which has local optima but can be solved by a greedy algorithm

2.2 Multimodal benchmark problems

Li et al. [16] lists several multimodal multi-objective problems. Many of them have a small number of decision valuables, such as Omni-test [5], SYM-PART [21], TWO-ON-ONE [20], and Polygon problems [10]. In contrast, The 3BC is scalable, that is, our method can design multimodal problems with any dimension of the design space. Some problems proposed in Yue et al. [27], Multi-Polygon [12], MMMOP [17], and SMMOP [24] are scalable but our method is still valid because the 3BC can also have multiple local optima yet it has more precise multimodality. That is, the local Pareto sets of the 3BC are completely calculated, and furthermore, we can specify the connectivity between each basin as the landscape. Kerschke et al. [15] presented mixed sphere problems having multimodality as described in section 2.1.

2.3 Other existing benchmark problems

There are well-known benchmark problems used to evaluate the performance of evolutionary multi-objective optimization (EMO) algorithms. The ZDT test suite [30] and DTLZ test suite [6] are widely used test problems. The Pareto set can be analytically obtained. The present benchmark of ours has the advantage that one can specify the local (and global) Pareto set more flexibly. In the ZDT and DTLZ, one could only change the Pareto set along the direction of the distance variables. The position variables parameterize the Pareto set. The numbers of distance and position variables could not be changed.

Huband et al. [9] proposed the WFG test suite to improve the ZDT and DTLZ test problems. The number of distance and position variables can be changed. The WFG possesses non-separability [9], and its Pareto front is known. The limitation of the WFG, however, is the difficulty in tuning multiple properties of the benchmark and in controlling the Pareto set. These are interdependent, and the Pareto set cannot be explicitly defined. For example, the test problem WFG3, which was expected to have the degenerate Pareto front, actually was found to have a non-degenerate part in the Pareto front [11]. An inverted version of DTLZ and WFG has been proposed [13, 14], yet the problem remains. The 3BC can be seen as an improvement to the WFG that offers an explicit control of characteristics and Pareto sets simultaneously and independently. With the 3BC we can create non-separable problems, and problems with various shapes of the Pareto front.

There are other commonly used test problems such as MaF [3], LSMOP [2], and UF [28]. MaF offers test problems with shapes of the Pareto front which do not appear in ZDT and DTLZ, and WFG. The LSMOP test problems are designed to evaluate the performance of large-scale EMO algorithms and the UF test suite has the advantage that their Pareto set and Pareto front are computed.

Other trends of standard benchmarking include COCO bbob-biobj [7], which contains 55 bi-objective problems, and a collection of real-world problems for benchmarking proposed by Tanabe et al. [23].

Our method can also make large-scale test problems with various shapes of Pareto fronts and, unlike all the above problems, has user-defined local Pareto sets and fronts.

3 Our multimodality: basin configuration

We model the multimodality suitable to our motivation. For this, we consider the *basins of attractions* [19].

Any point in the design space may reach multiple local Pareto sets without any component of the objective function increasing. Suppose, for example, x is a point in design space and it can reach two different components S_1 and S_2 of the local Pareto set by continually improving the values. Then some point in S_1 can arrive at another point in S_2 by increasing the value only at the point x. From this point of view, we can consider two components S_1 and S_2 connect each other. In the present paper, we would like to construct a benchmark problem corresponding to the given connectivity of components of the local Pareto sets. We consider this type of connection between the components by using some graph called the *basin graph*. For more details, see section 4.2 and section 5.4.

4 Characteristics of our benchmark

Our benchmark problem has characteristics that are guaranteed by the design and mathematical formulation. They can be configured by supplying a graph structure called the basin graph as input.

4.1 Overview

Graph input The benchmark problem is generated from the user-supplied basin graph that encodes information such as the positions of local Pareto efficient points and the connectivity of the basins of attraction. First, we consider a diamond.

Explicit positioning of local and global Pareto optima We allow the user to specify the positions of local and global Pareto optima. We provide the user with a series of candidate positions.

Multi-scaling in the design space The distance between a local Pareto optimum and the global Pareto optima is a simple example of this. The user can place local Pareto optima close and distant to each other, in different spatial scales. See section 5.2 for how we achieve this.

Scalability Computing the objective functions takes $O(dv)$ steps, where d is the dimension of the design space and v is the number of connected components of local minima lying in the design space.

4.2 Basin graph

We model the effects of basins using a hypothetical solver. Suppose we have a simple solver that improves the solution locally. This hypothetical solver checks the surroundings of distributed sample points and improves them by moving the sample points for an infinitesimal amount. More precisely, given a point in the design space, the movement of our hypothetical solver is restricted so that the direction only either improves or does not change f_i for any i. In our model, the basin attracts this hypothetical solver, trapping them in the local Pareto set. An actual solver, of course, has sophisticated mechanisms to do a global search for the global Pareto set. Due to this, the neighborhood of each point in the domain space is partitioned into parts, each of them can either be entered or not by this solver and leads to different connected components of the local Pareto set. The simplistic solver continues to move its sample point, to eventually find a local (or global) Pareto set. The potential paths of the solver can be summarized into a graph that describes the different paths from a starting point. In fact, we can merge the graphs for different starting points into one, which is called the basin graph.

s

4.3 Design details

In a sense, the 3BC aligns with the Exploratory Landscape Analysis (ELA) [18] in the sense that the landscape will be known. Where the ELA analyzes the landscape through a sample of points, the 3BC has a pre-defined landscape specified by the user as the basin graph we will explain later.

Our approach to realize a function from a user-specified topology has its root in visualization [26], although they targeted scalar functions while our method targets a mapping with a 2 dimensional range.

Our approach to the benchmark problem is similar to combining spheric functions, which is routinely done in the literature. Instead of the traditional sphere, i.e. $\{x \in X \mid \|x\|_2 < r\}$ for some radius $r > 0$ and some spatial domain X, we choose a version with the Manhattan distance, $\{x \in X \mid \|x\| < r\}$. By choosing this, we are able to specify the intersection of the spheres in X more easily, which in turn lets us fine-tune the benchmark problem.

We design our benchmark problem by splitting them into a few steps:

1. Generate a primitive uni-objective problem

2. Generate a primitive multi-objective problem

While each step is explained formally in later sections, here we provide some design decisions, mentioning how we fulfill the characters listed in section 4.1.

As in the list above, our first step is to construct a simple uni-objective optimization problem, then proceed to a multi-objective one (which is still simplistic) and finally morphing it into a more complex, final multi-objective optimization problem, which will be fed to the solvers to be benchmarked.

In step 1, we construct a uni-objective function f, which we call a *primitive function.* It is parameterized by a variable $t \geq 0 \in \mathbb{R}$. Hence, $f\colon [0,\infty) \times X \to \mathbb{R}$, where X is an n-dimensional domain specified later in eq. (2) as a disk. The objective function f can be regarded as a family $\{f_t\}_{t\geq 0}$ of objective functions $X \to \mathbb{R}$ by defining $f_t(x) \coloneqq f(t,x)$. At $t = 0$, the function $f_t\colon X \to \mathbb{R}$ is the zero function and at $t = 1$, f_t has a single local optimal (in fact, the minimum) solution. As we proceed in t, occasionally new local minima appear (see fig. 2). The user can give an ordering to the values of these local minima to decide the global minima.

In the domain space of f, $[0,\infty) \times X$, we thus have local minima each along a line parallel to the t-axis (see fig. 3). These locally minimal points will be the local Pareto optima of the resulting 2-objective problem in step 2. They will be moved in step 3, although the topology of the lines of these points stays the same. The function f in fig. 2 has two components of local minima and then their basins are described as in fig. 5.

In step 2, we construct a 2-objective problem $[0,\infty) \times X \ni (t,x) \mapsto (t, f(t,x)) \in \mathbb{R}^2$. Then we get each f_t as a slice of this 2-objective function at $t \in [0,\infty)$ (see fig. 4). We obtain $\tilde{f}$ by rotating the 2-objective function for 45° clockwise to have the desirable Pareto set and Pareto front:

$$\tilde{f}(t,x) \coloneqq \frac{1}{\sqrt{2}} \begin{pmatrix} 1 & 1 \\ -1 & 1 \end{pmatrix} \begin{pmatrix} t \\ f(t,x) \end{pmatrix}. \tag{1}$$

The final problem is obtained as follows. We can make the Pareto set of the problem in step 2 more complicated, which would reduce the performance of solves. We can also deform the shape of the Pareto front, which has an effect on the performance of algorithms because a different algorithm is good at a different shape of the Pareto front.

Characteristics of our benchmark problem can be explained by the condition on the critical values m_s's of f, which will appear in appendix A. For example, Separability is achieved if $m_\emptyset$ is the minimum of m_s's. The critical values m_s's also determine the shape of Pareto front and especially the Pareto front is completely convex when $m_\emptyset$ is the minimum of m_s's.

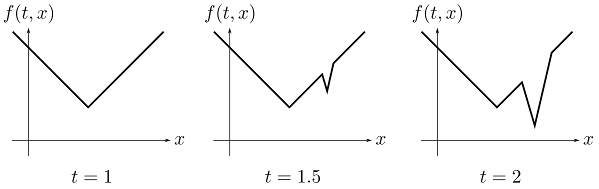

Figure 2: Graphs of f_t's ($\dim X = 1$)

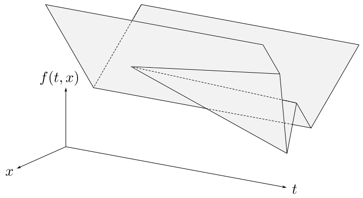

Figure 3: Graph of f ($\dim X = 1$)

5 Overview of the primitive function f

5.1 Property of the primitive function f

As mentioned in section 4.3, we regard $f\colon [0,\infty) \times X \to \mathbb{R}$ as a family $\{f_t\}_{t\geq 0}$ of single-objective functions on X such that local minima are added as t increases. In this section, we explain what properties we request for f. First, the domain X is defined to be the unit ball in $\mathbb{R}^n$ whose shape is like a diamond, that is,

$$X = \{x \in \mathbb{R}^n \mid \|x\| \leq 1\}, \tag{2}$$

where $\|x\| = \sum_{i=1}^{n} |x_i|$ is the norm of x. Then X is the black diamond on the left of fig. 6. When $t = 1$, we construct f so that it has only one local minimum at the origin. When t increases and reaches 2, the function f_t can have more local minima other than the origin. Each local minimum has its diamond in which the function has only one local minimum, for example, the two red diamonds in the middle figure in fig. 6). The specific definition of the diamond is given in section 5.2, in particular in (4). Similarly, f_3 may have more local minima other than those of f_2.

5.2 Positioning local minima and their diamond

Local minima of the primitive function f can be chosen from predefined candidate positions. To allow the benchmark to model multiple scales in the design space, we place the position in a fractal structure (see fig. 7). The position of each candidate point is coded as a sequence s of *movements*. We start with the origin of the coordinate system and follow the movements coded in s to specify the candidate position x_s. Each j-th movement can be taken along an axis in X, and it can either go backwards or forwards for length $2/4^j$. In addition, a movement can also stay at the position. We denote each

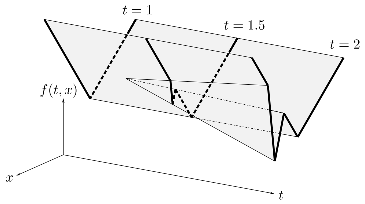

Figure 4: Family $\{f_t\}_t$ as slices of f ($\dim X = 1$)

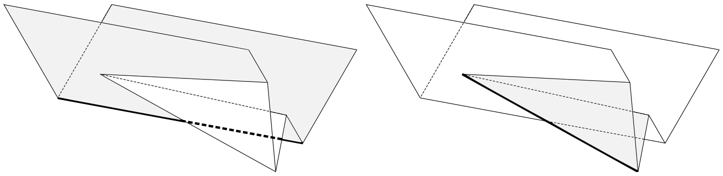

(a) Basin of first minimum (b) Basin of second minimum

Figure 5: Basins of local minima

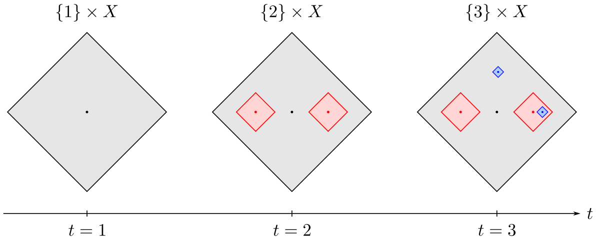

Figure 6: An example of diamonds in X ($n = \dim X = 2$)

movement along i-th axis backwards or forwards as i^- and i^+, respectively. In addition, a "movement" can also be a *stay*, indicated by a 0, and so we can write down a sequence s of movements as, e.g.,

$$s \coloneqq 1^+ \, 0 \, 2^+. \tag{3}$$

This example results at the position illustrated in fig. 7. We require the last movement of any sequence not to be 0. In the example indicated in fig. 6, the appearing movements are $s = \emptyset$, 1^+, 1^-, $1^+ \, 1^+$, and $0 \, 2^+$.

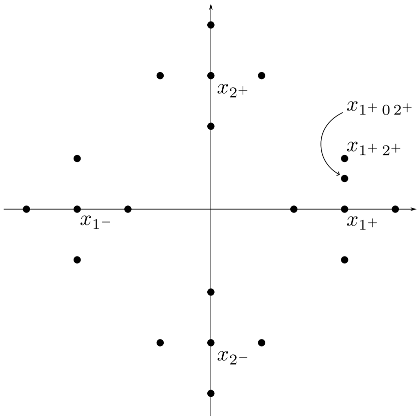

Figure 7: Position of local minima ($\dim X = 2$)

We denote the number of movements in s as $|s|$ (= 3 for eq. (3)). We allow $s = \emptyset$, which denotes a local minimum at the origin. Indeed, this local minimum is a mandatory user input in our benchmark for the sake of simpler mathematics. The user specifies the position of the local minimum with a sequence of movements.

For each s, its diamond $D_s \subset X$ is defined by

$$D_s = \{x \in X \mid \|x - x_s\| \leq 1/4^{|s|}\}. \tag{4}$$

Then diamonds of movements of the same length are all disjoint. Let s be a movement and consider its "child" $s' = sj^{\pm}$ for some $1 \leq j \leq n$. Since $\|x_s - x_{s'}\| = 2/4^{|s|+1}$, the diamond of s' is a subset of that of s, which means the diamonds are nested.

5.3 Parameter-family of local optima as local Pareto set

By increasing t, we give rise to new local minima of f, which will be the local Pareto optima of the 3BC. We assume f to be continuous for the sake of the simplicity of the mathematics. Each local minimum at position x_s emerges right after $t = |s|$, having the local minimum value $M_s(t)$ and reach the user-specified value m_s at $t = |s| + 1$. After this t, the local minimum stays constant at this value, and will stay being a local minimum. The precise definition of $M_s(t)$ appears in section 6.2 and its graph is on the left side of fig. 9. As in fig. 9, the set $\{(t, x_s) \mid t \geq |s|\}$, which is the component of local minima of f for node s, is also a connected component of the local Pareto sets of $\tilde{f}$ if

$$m_s - f(|s|, x_s) > -1.$$

Otherwise the connected component is $\{(t, x_s) \mid t \geq |s| + 1\}$, that is, each point in the set $\{(t, x_s) \mid |s| \leq t \leq |s| + 1\}$ is not a local optimum (see red lines in fig. 9). Note that m_s must satisfy more preliminary condition (6) appearing later to be a local minimum of f.

5.4 Specifying basins using the basin graph

Recall that the user specifies the position of a local minimum using a sequence of movements as in eq. (3). This defines a tree structure, which we call the *basin graph.* Our basin graph is similar to the *reachability graph* [1] Each node corresponds to a movement, which in turn corresponds to a connected component of the local minima of f. – the root node of this tree corresponds to the local minimum without a movement, i.e. $s = \emptyset$. Let s be the sequence of movements for a node in the tree. This node is connected to a child node with a link if and only if (i) s matches the first $|s|$ items in the sequence of the child node, and (ii) the child node is not an offspring of another child of this parent node. We call the local minimum corresponding to the parent and child basins simply a *parent* or a *child.*

By using the basin graph, the basin of each node can be defined as follows. For a node s, from its diamond D_s we obtain

$$\bigcup_{t \geq |s|} \{t\} \times D_s,$$

which shapes a cone since the radius of the diamond increases monotonically. Then, the basin of a node is defined as its cone subtracted by cones of all children of the node.

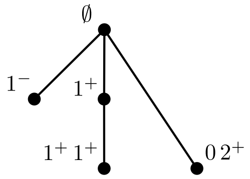

Figure 8: The basin graph corresponding fig. 6

6 Defining and computing the primitive function f

We define the objective function f for $t = 0$ and then $t > |s|$ inside the diamond

$$D_s = \{x \in X \mid \|x - x_s\| \leq 1/4^{|s|}\} \tag{4}$$

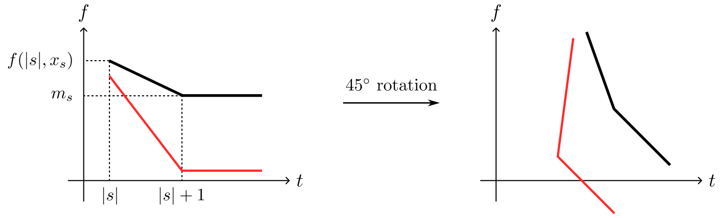

Figure 9: Local minima of f and a local Pareto front of $\tilde{f}$

of each s. As the domain of f is restricted to the largest diamond (eq. (2)) for at any t, f is indeed assigned value at any point. If a point is inside two diamonds of sequences s_1 and s_2, we choose f defined by the cone of the younger s_i (i.e. the one with larger $|s_i|$).

In the next two sections, we will define $f\colon [0,\infty) \times X \to \mathbb{R}$ by inductively constructing $f\colon (\tau, \tau + 1] \times X \to \mathbb{R}$ for $\tau = 0, 1, 2, \ldots$

6.1 At $t = 0$

Let x be a point in X. We define $f(t, x)$ as

$$f(t, x) \coloneqq 0 \quad \text{for } t = 0.$$

6.2 At $\tau < t \leq \tau + 1$.

Assuming that f is defined for $\{\tau\} \times X$, where τ is a non-negative integer, we construct f for $(t, x) \in (\tau, \tau + 1] \times X$ in the following manner. We consider the sequences of movements whose length is τ (if they exist in the user input). Let s (with $|s| = \tau$) be such one. If there is none, $f(t, x) \coloneqq f(\tau, x)$ for any $x \in X$.

In the remainder, we consider the situation when such a sequence s exists. Let S_τ be the set of such sequences. If so, $f(t, x)$ for $(t, x) \in (\tau, \tau + 1] \times X$ is defined to be

$$f(t, x) \coloneqq \min_{|s|<t} \{g_s(t, x)\}. \tag{5}$$

(see fig. 2). The function g_s is explained in the rest of this subsection.

As shown in fig. 10, the locally minimum value $M_s(t)$ at position x_s firstly appears right after $t = \tau$, decreasing its value to the user-given m_s via linear interpolation, till $t = \tau + 1$:

$$M_s(t) \coloneqq (1 - \Delta t)\ f(\tau, x_s) + \Delta t\ m_s,$$

where $\Delta t \coloneqq \min(t - \tau, 1)$ and $t \geq \tau$. min is taken to stop the growth of $g_s(t, x)$ at $t = \tau + 1$ and we impose the following condition on m_s's specified by the user.

$$m_s < f(|s|, x_s). \tag{6}$$

Function value $g_s(t, x)$ at parameter t on a point x around the local minimum point x_s is given by climbing upwards from x_s, following the gradient vector $\nabla g_s(x)$:

$$g_s(t, x) \coloneqq M_s(t) + \nabla g_s(x) \cdot \Delta x, \tag{7}$$

where $\Delta x \coloneqq x - x_s$ is a vector expressing the deviation from the locally minimal point.

To decide $\nabla g_s(x)$, we compute the intersection points between the graphs of s and the parent of s (see fig. 11). Note that $\nabla g_s(x)$ is independent of t.

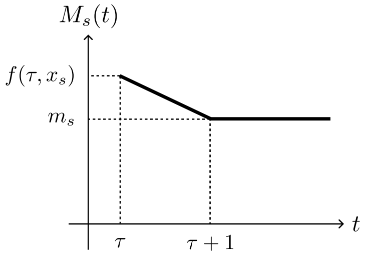

Figure 10: Value of f at a local minimum x_s.

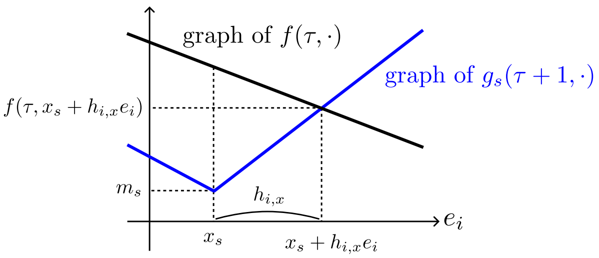

graph of $f(\tau, \cdot)$
graph of $g_s(\tau + 1, \cdot)$
$f(\tau, x_s + h_{i,x} e_i)$
m_s
$h_{i,x}$
e_i
x_s
$x_s + h_{i,x} e_i$

Figure 11: Definition of $\nabla g_s(x)$

We require any, say i-th, component of $\nabla g_s(x)$ to match

$$\frac{f(\tau + 1,\ x_s +\ h_{i,x}\ e_i) - f(\tau + 1,\ x_s)}{h_{i,x}} =: \nabla g_s^i(x), \tag{8}$$

which follows from the definition of a differential. Here, e_i is the i-th unit vector and $x_s + h_{i,x}\ e_i$ gives location of $x \in X$ at which the graph of $g_s(t, x)$ intersects $f(\tau, \bullet)$:

$$h_{i,x} \coloneqq \operatorname{sgn}(i, x) \frac{1}{4^\tau} \ \in \mathbb{R}.$$

$\operatorname{sgn}(i, x)$ tells the side of the diamond on which point x lies along the i-th axis, i.e. the sign of $x^i - x_s^i$. If this subtraction tends to 0 (or, $x^i \to x_s^i$), $\nabla g_s^i(x) \times (x^i - x_s^i)$ in eq. (7) approaches 0, regardless of the value of sgn. In our implementation, we thus set $\operatorname{sgn}(i, x_s)$ simply to 1.

In fact, regarding eq. (8), $f(t,\ x_s +\ h_{i,x}\ e_i)$ is constant as the $x_s +\ h_{i,x}\ e_i$ is outside the diamond of s. In addition, $f(\tau + 1,\ x_s) = m_s$ because x_s is the local minimum point. Hence,

$$\nabla g_s^i(x) \equiv \frac{f(\tau,\ x_s +\ h_{i,x}\ e_i) - m_s}{h_{i,x}},$$

and we can determine g_s using eq. (7).

Finally, we decide $f\colon (\tau, \tau + 1] \times X \to \mathbb{R}$:

$$f(t, x) \coloneqq \min_{|s|<t} g_s(t, x) = \min\left(\{f(\tau, x)\} \cup \{g_s(t, x) \mid |s| = \tau\}\right).$$

The first equality is due to eq. (5).

$$\begin{aligned} f(t, x) &= \min_{|s| \le \tau} g_s(t, x) \\ &= \min(\{g_s(t, x) \mid |s| \le \tau - 1\} \cup \{g_s(t, x) \mid |s| = \tau\}) \\ &= \min(\{g_s(\tau, x) \mid |s| \le \tau - 1\} \cup \{g_s(t, x) \mid |s| = \tau\}) \\ &= \min(\{f(\tau, x)\} \cup \{g_s(t, x) \mid |s| = \tau\}) \end{aligned}$$

As shown in fig. 11, and by equation 7, for $t \in (\tau, \tau+1]$ and a sequence s with $|s| = \tau$, $g_s(t,x) \leq f(\tau, x)$ only in the diamond of s. The function f_τ does not have x_s as a critical point, but g_s does for every t, so minimization above can make x_s a critical point after $t \geq \tau$. It is our desirable condition.

7 Basin-Wise IGDX

It is useful to measure whether each solver finds the optimal solutions. We can use various performance indicators such as GD [25], IGD [4], GDX [22], and IGDX [22, 29] to do it since the Pareto set and front of our benchmark problem are known. Hypervolume [31] is also useful.

3BC is designed to study the behavior of Evolutionary Algorithms (EAs) that change at each generation, reacting to the basins. As a result, we study the population at each generation of different EAs such as GDE, IBEA etc. In other words, we do not use the external archive for our evaluation of the 3BC – such a strategy is more suited for studying the overall performance of EAs instead of the reaction to the basins for the situation EAs is in at the temporal instant.

It is also useful to measure whether solutions obtained by a solver is close to the local Pareto sets or not. The IGDX is also useful here by taking P^* (this notation appears below) as a subset of the local Pareto sets. However, the IGDX can take a good value even when solutions obtained by an algorithm are distributed all over the place. It can be improved by combining the IGDX above with the GDX since the more solutions obtained by an algorithm away from the local optima, the worse the GDX.

These indicators cannot measure how much the solver is misled by each local optimum along the way, so another performance indicator is needed to measure that. One conventional way to measure the extent to which a solver is trapped in a local Pareto solution is to use x-means. This is simply a measure of how many clusters it is appropriate to divide the solver's solution into. In contrast, the 3BC defines the basin of attraction for each node (connected component of the local Pareto set). We can be use it to define an indicator for each basin, which we call a *basin-wise* indicator for each basin. In particular, *basin-wise* IGDX for each basin of attraction can measure how much a solver's solution falls into its basin.

Let P be the solution by a solver and P^* be the (global) Pareto set. Then original IGDX is defined by

$$\mathrm{IGDX}(P^*, P) = \frac{\Sigma_{v \in P^*} d(v, P)}{|P^*|},$$

where $d(v, P)$ is the Euclidian distance in the decision space. Replacing P^* by a local Pareto optimum may define a IGDX for the basin but this indicator has an undesirable property: The situation where the solutions P is stuck in other basins has an unintended effect on the value of the indicator. This is due to the fact that the entire solution is taken as P, and it would be a good indicator if we focus only on the solutions related to the basin. In general, it is not possible to do so, but 3BC has a basin of attraction, which can be defined. That is, we define basin-wise IGDX for a node P^* by the value

$$\mathrm{IGDX}(P^*, B) = \frac{\Sigma_{v \in P^*} d(v, B)}{|P^*|},$$

where B is the basin of P^*.

8 Evaluation

When an algorithm solves the 3BC, the values of basin-wise IGDX in each generation construct a line graph. For example, consider a 3BC having a basin graph in fig. 12a, which we call a depth-base basin graph. This 3BC has five nodes $\emptyset$, $1^+\,1^+$, $1^+\,1^+\,1^+$, $1^+\,1^+\,1^+\,1^+$, and $1^+\,1^+\,1^+\,1^+\,1^+$.

Let the values m_s's be -1, -2, -3, -4, and -5. The line graphs of the basin-wise IGDX are as shown in fig. 13, where the solvers are GDE, IBEA, MOEA/D, NSGA-II, and OMOPSO.

For another example, we take a basin graph illustrated in fig. 12b, which we call a breadth-base basin graph. This 3BC has five nodes $\emptyset$, 1^+, 1^-, 2^+, and 2^-. As with the depth-base 3BC, label these nodes in order from 0 to 4. For this 3BC, the line graphs of the basin-wise IGDX for each node are shown in fig. 14.

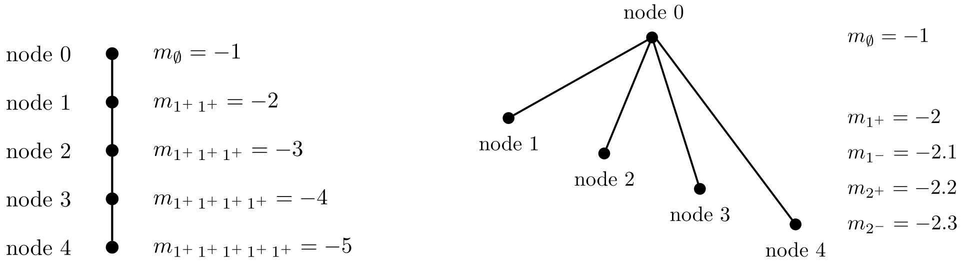

(a) A depth-base basin graph

(b) A breadth-base basin graph

Figure 12: Examples of the basin graph

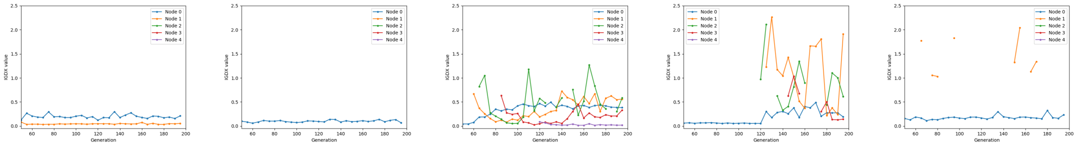

(a) GDE

(b) IBEA

(c) MOEA/D

(d) NSGA-II

(e) OMOPSO

Figure 13: Basin-wise IGDX for each basin of attraction (for a depth-base basin graph)

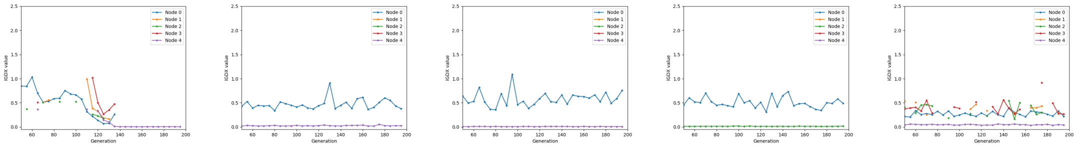

(a) GDE

(b) IBEA

(c) MOEA/D

(d) NSGA-II

(e) OMOPSO

Figure 14: Basin-wise IGDX for each basin of attraction (for a breadth-base basin graph)

Comparing the graphs for the depth-base and breadth-base 3BCs in fig. 13 and fig. 14, we can find the following differences in performance of each solver for depth-base and breadth-base 3BCs, which implies 3BCs for different basin graphs have different properties as multimodal multi-objective benchmark problems.

1. GDE can only find node 1 for the depth-base 3BC, but can find the node 4 (global optima) for the breadth-base 3BC in around 130th generation.

2. IBEA cannot find any node other than node 0 for the depth-base 3BC, but can find the global optima for the breadth-base 3BC.

3. MOEA/D can find global optima and also find other local optima for the depth-base 3BC, and almost all generation points are located in the basin of the node 4 for the depth-based 3BC.

4. NSGA-II cannot find (local) optima by the 200th generation for the depth-base 3BC, but is trapped in the basin for node 2 for the breadth-base 3BC.

5. OMOPSO cannot find any node other than node 0 for the depth-base 3BC, but can find the global optima for the breadth-base 3BC.

9 Conclusion

We have proposed a novel benchmark problem suite called the 3BC, which has an explicitly definable multimodal landscape with an arbitrary dimensional design space. Our work employs the basin graph for generating the problem. By utilizing our benchmark problem, one can now define the positions as well as the value of the optima for benchmarking a multi-objective optimization solver. Additionally, our benchmark problem can be set to be non-separable.

A On separability and shape of the Pareto front

Separability Both separable and non-separable problems can be obtained by our method. A solver can detect a Pareto optimum in a separable problem just by optimizing each parameter individually [8]. Hence, non-separability is one of the properties required for complex benchmark problems. Our benchmark is non-separable if $m_\emptyset$ is not the minimum among m_s's proved in the following.

The definition of separability [9] is the following. Let O be a single objective optimization problem with design valuables x_i's. For each index i we can consider a single objective and single variable problem $P_{O,\mathbf{x},i}$ from O by fixing a parameter $\mathbf{x}$ of the design space and varying only x_i. Then x_i is said to be *separable* on O if the set of the global optima $P^*_{O,\mathbf{x},i}$ of $P_{O,\mathbf{x},i}$ is the same for any parameter x. The optimization problem O is said to be *separable* if every x_i is separable on O. Morerover, a multi-objective optimization problem is said to be *separable* if every objective of the problem is separable.

One necessary condition for our benchmark problem being separable is that $m_\emptyset$ is the minimum along all m_s's. $\tilde{f}$ is defined by (1).

$$\tilde{f}(t,x) := \frac{1}{\sqrt{2}}\begin{pmatrix} 1 & 1 \\ -1 & 1 \end{pmatrix}\begin{pmatrix} t \\ f(t,x) \end{pmatrix}. \tag{1}$$

Since $\tilde{f}$ is separable, the first component $\frac{1}{\sqrt{2}}(t+f(t,x))$ is separable. That each parameter x_i is separable on this component means that x_i is separable on f. For each i, $P_{f,(1,x),i} = |x_i| + \text{constant}$, where $x = (1/4, 0, \ldots, 0)$ if $i \neq 1$ and $x = (0, 1/4, 0, \ldots, 0)$ if $i = 1$. Hence $P^*_{f,(1,x),i} = \{0\}$. The separability of f implies that

$$P^*_{f,(t,x),i} = \{0\}$$

for any (t,x) and i. Now we prove that $m_\emptyset$ is the minimum. Take $t_0 > 0$ large enough for $f(t_0, x_s) = m_s$ for every node s. Let $x_s = (y_1, \ldots, y_n) \in \mathbb{R}^n$ be the coordinates of x_s. By using (A) n times, we have

$$\begin{aligned} m_s &= f(t_0, y_1, \ldots, y_n) \\ &\geq f(t_0, y_1, \ldots, y_{n-1}, 0) \\ &\geq f(t_0, y_1, \ldots, y_{n-2}, 0, 0) \\ &\ldots \\ &\geq f(t_0, 0, \ldots, 0) \\ &= m_\emptyset. \end{aligned}$$

Hence $m_\emptyset$ is the minimum.

Concave-ity of the Pareto optimal shape The shape of a Pareto front often affects the performance of solvers. Each local Pareto front of our benchmark is convex (illustrated in fig. 9). The Pareto front, which is the combination of local Pareto fronts, is generally a mix of linear, convex, and concave fronts.

References

[1] Jan Bormann, Lars Huettenberger, and Christoph Garth, *The approximation of pareto sets using directed joint contour nets*, Topological Methods in Data Analysis and Visualization V (Cham) (Hamish Carr, Issei Fujishiro, Filip Sadlo, and Shigeo Takahashi, eds.), Springer International Publishing, 2020, pp. 173–185.

[2] Ran Cheng, Yaochu Jin, Markus Olhofer, et al., *Test problems for large-scale multiobjective and many-objective optimization*, IEEE Transactions on Cybernetics **47** (2016), no. 12, 4108–4121.

[3] Ran Cheng, Miqing Li, Ye Tian, Xingyi Zhang, Shengxiang Yang, Yaochu Jin, and Xin Yao, *A benchmark test suite for evolutionary many-objective optimization*, Complex & Intelligent Systems **3** (2017), no. 1, 67–81.

[4] Carlos A Coello Coello and Margarita Reyes Sierra, *A study of the parallelization of a coevolutionary multi-objective evolutionary algorithm*, MICAI 2004: Advances in Artificial Intelligence: Third Mexican International Conference on Artificial Intelligence, Mexico City, Mexico, April 26-30, 2004. Proceedings 3, Springer, 2004, pp. 688–697.

[5] Kalyanmoy Deb, *Multi-objective genetic algorithms: Problem difficulties and construction of test problems*, Evolutionary computation **7** (1999), no. 3, 205–230.

[6] Kalyanmoy Deb, Lothar Thiele, Marco Laumanns, and Eckart Zitzler, *Scalable test problems for evolutionary multiobjective optimization*, Evolutionary multiobjective optimization, Springer, 2005, pp. 105–145.

[7] N. Hansen, A. Auger, R. Ros, O. Mersmann, T. Tušar, and D. Brockhoff, *COCO: A platform for comparing continuous optimizers in a black-box setting*, Optimization Methods and Software **36** (2021), 114–144.

[8] Simon Huband, Luigi Barone, Lyndon While, and Phil Hingston, *A scalable multi-objective test problem toolkit*, International Conference on Evolutionary Multi-Criterion Optimization, Springer, 2005, pp. 280–295.

[9] Simon Huband, Philip Hingston, Luigi Barone, and Lyndon While, *A review of multiobjective test problems and a scalable test problem toolkit*, IEEE Transactions on Evolutionary Computation **10** (2006), no. 5, 477–506.

[10] Hisao Ishibuchi, Naoya Akedo, and Yusuke Nojima, *A many-objective test problem for visually examining diversity maintenance behavior in a decision space*, Proceedings of the 13th annual conference on Genetic and evolutionary computation, 2011, pp. 649–656.

[11] Hisao Ishibuchi, Hiroyuki Masuda, and Yusuke Nojima, *Pareto fronts of many-objective degenerate test problems*, IEEE Transactions on Evolutionary Computation **20** (2015), no. 5, 807–813.

[12] Hisao Ishibuchi, Yiming Peng, and Ke Shang, *A scalable multimodal multiobjective test problem*, 2019 IEEE congress on evolutionary computation (CEC), IEEE, 2019, pp. 310–317.

[13] Hisao Ishibuchi, Yu Setoguchi, Hiroyuki Masuda, and Yusuke Nojima, *Performance of decomposition-based many-objective algorithms strongly depends on pareto front shapes*, IEEE Transactions on Evolutionary Computation **21** (2017), no. 2, 169–190.

[14] Himanshu Jain and Kalyanmoy Deb, *An improved adaptive approach for elitist nondominated sorting genetic algorithm for many-objective optimization*, Evolutionary Multi-Criterion Optimization (Berlin, Heidelberg) (Robin C. Purshouse, Peter J. Fleming, Carlos M. Fonseca, Salvatore Greco, and Jane Shaw, eds.), Springer Berlin Heidelberg, 2013, pp. 307–321.

[15] Pascal Kerschke, Hao Wang, Mike Preuss, Christian Grimme, André Deutz, Heike Trautmann, and Michael Emmerich, *Towards analyzing multimodality of continuous multiobjective landscapes*, Parallel Problem Solving from Nature–PPSN XIV: 14th International Conference, Edinburgh, UK, September 17-21, 2016, Proceedings 14, Springer, 2016, pp. 962–972.

[16] Wenhua Li, Tao Zhang, Rui Wang, Shengjun Huang, and Jing Liang, *Multimodal multi-objective optimization: Comparative study of the state-of-the-art*, Swarm and Evolutionary Computation (2023), 101253.

[17] Yiping Liu, Gary G Yen, and Dunwei Gong, *A multimodal multiobjective evolutionary algorithm using two-archive and recombination strategies*, IEEE Transactions on Evolutionary Computation **23** (2018), no. 4, 660–674.

[18] Olaf Mersmann, Bernd Bischl, Heike Trautmann, Mike Preuss, Claus Weihs, and Günter Rudolph, *Exploratory landscape analysis*, Proceedings of the 13th annual conference on Genetic and evolutionary computation, 2011, pp. 829–836.

[19] Mike Preuss, *Multimodal optimization by means of evolutionary algorithms*, Springer, 2015.

[20] Mike Preuss, Boris Naujoks, and Günter Rudolph, *Pareto set and emoa behavior for simple multimodal multiobjective functions*, International Conference on Parallel Problem Solving from Nature, Springer, 2006, pp. 513–522.

[21] Günter Rudolph, Boris Naujoks, and Mike Preuss, *Capabilities of emoa to detect and preserve equivalent pareto subsets*, Evolutionary Multi-Criterion Optimization: 4th International Conference, EMO 2007, Matsushima, Japan, March 5-8, 2007. Proceedings 4, Springer, 2007, pp. 36–50.

[22] Oliver Schutze, Massimiliano Vasile, and Carlos A Coello Coello, *Computing the set of epsilon-efficient solutions in multiobjective space mission design*, Journal of Aerospace Computing, Information, and Communication **8** (2011), no. 3, 53–70.

[23] Ryoji Tanabe and Hisao Ishibuchi, *An easy-to-use real-world multi-objective optimization problem suite*, Applied Soft Computing **89** (2020), 106078.

[24] Ye Tian, Ruchen Liu, Xingyi Zhang, Haiping Ma, Kay Chen Tan, and Yaochu Jin, *A multi-population evolutionary algorithm for solving large-scale multimodal multiobjective optimization problems*, IEEE Transactions on Evolutionary Computation **25** (2020), no. 3, 405–418.

[25] David Allen Van Veldhuizen, *Multiobjective evolutionary algorithms: classifications, analyses, and new innovations*, Air Force Institute of Technology, 1999.

[26] Gunther Weber, Peer-Timo Bremer, and Valerio Pascucci, *Topological landscapes: A terrain metaphor for scientific data*, IEEE Transactions on Visualization and Computer Graphics **13** (2007), no. 6, 1416–1423.

[27] Caitong Yue, Boyang Qu, Kunjie Yu, Jing Liang, and Xiaodong Li, *A novel scalable test problem suite for multimodal multiobjective optimization*, Swarm and Evolutionary Computation **48** (2019), 62–71.

[28] Qingfu Zhang, Aimin Zhou, Shizheng Zhao, Ponnuthurai Nagaratnam Suganthan, Wudong Liu, Santosh Tiwari, et al., *Multiobjective optimization test instances for the cec 2009 special session and competition*, University of Essex, Colchester, UK and Nanyang technological University,

Singapore, special session on performance assessment of multi-objective optimization algorithms, technical report **264** (2008), 1–30.

[29] Aimin Zhou, Qingfu Zhang, and Yaochu Jin, *Approximating the set of pareto-optimal solutions in both the decision and objective spaces by an estimation of distribution algorithm*, IEEE Transactions on Evolutionary Computation **13** (2009), no. 5, 1167–1189.

[30] Eckart Zitzler, Kalyanmoy Deb, and Lothar Thiele, *Comparison of multiobjective evolutionary algorithms: Empirical results*, Evolutionary Computation **8** (2000), no. 2, 173–195.

[31] Eckart Zitzler and Lothar Thiele, *Multiobjective optimization using evolutionary algorithms—a comparative case study*, International conference on parallel problem solving from nature, Springer, 1998, pp. 292–301.